One-pot synthesis of Mo_2C&MoS_2 loaded on N/S co-doped carbon materials as the electrocatalyts for hydrogen evolution reation

Qichang Wang[a], Ran Yu[a], Dekui Shen[a*], Guofu Liu[b*], Kai Hong Luo[c], Chunfei Wu[d], Sai Gu[e]

[a] Key Laboratory of Energy Thermal Conversion and Control of Ministry of Education, School of Energy and Environment, Southeast University, Nanjing 210096, Jiangsu, PR China

[b] School of Energy and Power Engineering, Qilu University of Technology (Shandong Academy of Sciences), Jinan, 250353, Shandong, China

[c] Department of Mechanical Engineering, University College London, London, WC1E 7JE, United Kingdom

[d] School of Chemistry and Chemical Engineering, Queen's University Belfast, Belfast, BT7 1NN, United Kingdom

[e] Faculty of Engineering and Physical Sciences, University of Surrey, Guilford, GU2 7XH, United Kingdom

* Corresponding author: * 101011398@seu.edu.cn (D. K. Shen), golfliu@qlu.edu.cn (Guofu Liu)

Abstract:

Biomass is a potential precursor for preparing functional carbon materials, as the organic component containing nitrogen (N), sulfur (S) would create the atomic dopants to adjust electronic properties of the carbon material. The heteroatom-doped carbon materials loaded with non-precious metal compound is considered to be a promising alternative for hydrogen evolution reaction (HER). Herein, Mo_2C and MoS_2 nanoparticles with a size of 5~20 nm uniformly loaded on the N/S-co-doped carbon sheets (NSC) are prepared via direct pyrolysis of ginkgo leaves with ammonium

molybdate tetrahydrate (AMT). Carbon black (CB) is used to replace ginkgo leaves to obtain $Mo_2C@NC_3$ to further study the influence of N/S-containing organic components in ginkgo leaves. By comparing with $Mo_2C@NC_3$, the XPS reflect the characteristic peak of Mo is positively shifted while the characteristic peak of N 1s is obviously negatively shifted, indicating a stronger electron interactions of $Mo_2C\&MoS_2@NSC_3$. Benefited from the intense electronics transfer, the efficiency electrochemical active areas of $Mo_2C\&MoS_2@NSC_3$ is larger than $Mo_2C@NC_3$ (10.72 *vs*. 4.97 mF/cm^{-2}), thus the $Mo_2C\&MoS_2@NSC_3$ gives a smaller overpotential of 209 mV to obtain the current density of 10 mA cm^{-2}, together with a low Tafel slope value of 85.5 mV dec^{-1}.

Keywords: $Mo_2C\&MoS_2$, N/S co-doped carbon, electrocatalysts, hydrogen evolution reaction, ginkgo leaves

1 Introduction

The huge energy demand and environmental pollution of human society enforce the exploration for alternatives of traditional energy. Hydrogen gas (H_2) is regarded as an efficient and pollution-free energy carrier, thus the methods for generating H_2 have been world-wide investigated [1-3]. Steam reforming of fossil resources is a commonly industrial method to produce H_2 but will result in the consuming of fossil fuel and emit carbon dioxide (CO_2) [4]. By contrast, electrolysis water splitting is an appealing strategy to obtain H_2 for its easy availability of raw materials and emission-free [5, 6]. Hydrogen evolution reaction (HER) is the cathode reaction during the water splitting. Among various electrocatalysts, platinum-group based catalysts (Pt, Pd, et al.) have the best activity to electrocatalytic HER due to its optimal hydrogen bonding energy [7, 8]. The high-cost and scarce reserves seriously limit the scalable application of noble metals in electrocatalytic H_2 production,

extensive efforts have been devoted to search the substitutes with earth-abundant sources [9-11]. According to the volcano plots, transition metals such as nickel (Ni), cobalt (Co) and molybdenum (Mo) are the idea alternatives for H_2 production [12-18]. The carbides of transition metal possess the Pt-like band structure which endow them to adsorb and activate hydrogen [19]. Molybdenum carbides (Mo_2C) have already been demonstrated similar chemistry peculiarity to Pt-group catalysts in catalyzing hydro-processing reaction [20, 21]. However, the poor conductivity and relative strong of hydrogen adsorption energy restrict the HER performance of Mo_2C [19, 22, 23]. The molybdenum sulfide (MoS_2) possesses moderate hydrogen bonding also suffers the low conductivity which serious restrict its catalytic activity for HER [24]. More than that, the typical lamellar crystal structure results in the violent aggregation which make against the active sites exposure [25, 26]. It is more sufficient to enhance the catalytic activity of Mo_2C and MoS_2 by loading it on a high conductivity matrix [27, 28].

Carbon-based matrix such as carbon nanotube, graphene and carbon fiber have been attracted many attentions for it satisfactory effect on promoting the electrons transfer [29-32]. Embedding the metal compounds on carbon support will benefit to downsize the size of metal particles and promote its uniform dispersion, thus benefit to expose more active sites [19]. The coupling of Mo_2C, MoS_2 and carbon has also been shown to be beneficial for optimizing the Mo-H bond strength [33, 34]. Especially, the carbon matrix doped with heteroatoms have been proven to further boost the HER performance of Mo_2C and MoS_2 by enhancing the catalytic activity of carbon atoms adjacent to doped atoms [19, 35]. While the typical techniques for manufacturing heteroatoms doped carbon are to introduce the exogenous heteroatoms sources (melamine [36], thiourea [37], etc.) into the

carbon matrix. The $Mo_2C\&MoS_2$ loaded carbon matrix is generally prepared via hydrothermal followed post-calcination method which is relative complex and with large energy consumption [33, 38]. Compared with such normal carbon materials, biomass is an abundant renewable source consisted of several organic contents containing the nitrogen (N), sulfur (S) and phosphorus (P) element, which can be introduced into the carbon skeleton as dopants during the biomass conversion [39, 40]. The plenty of surface functional group endow its with huge space to be functionalized and applicated in the electrocatalysis such as HER [41], oxygen evolution reaction (OER) [42-44], carbon dioxide reduction reaction (CO_2RR) [45, 46]. Furthermore, the nonmetal element may combine with metal to form metal compounds to enhance the catalytic activity which is taking full use of the pristine properties of biomass [16, 17].

Ginkgo trees are widely planted in the China as a landscape tree. The ginkgo leaves are rich in N and S element which make it is possible to be converted to N/S doped carbon via simple thermal treatment. Herein, as shown in scheme 1, the ginkgo leaves are chosen as the biomass precursor and mixed with ammonium molybdate tetrahydrate (AMT) by simply grounding. The AMT decomposed into ammonia (NH_3) and molybdenum trioxide (MoO_3) during the pyrolysis. The escape of NH_3 produce the addition N atoms. While the MoO_3 combined with the C and S to form the Mo_2C and MoS_2. The Mo_2C and MoS_2 nanoparticles with a size of 5~30 nm homogeneous dispersed on the N/S co-doped carbon sheets ($Mo_2C\&MoS_2$@NSC). As expect, the Mo_2C and MoS_2 serves as the efficient active sites and significantly enhance the HER performance for ginkgo leaves derived carbon materials. More than that, the activity of $Mo_2C\&MoS_2$@NSC is better than $Mo_2C@NC_3$ derived from carbon black and AMT, which have reflected the advantage of ginkgo

leaves as the precursor, that the heteroatom originated from ginkgo leaves play a critical role in electrocatalytic HER.

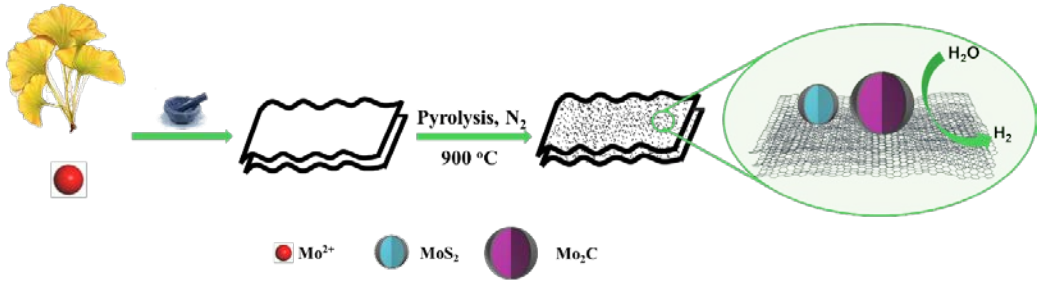

Scheme 1 Schematic illustration of the fabrication process of $Mo_2C\&MoS_2@NSC_x$.

2 Experiment

2.1 Materials

Ammonium molybdate tetrahydrate ($(NH_4)_6Mo_7O_{24}\cdot 4H_2O$, 99.99%, AMT), sodium molybdate ($Na_2MoO_4\cdot 2H_2O$), thiourea (CH_4N_2S), sulfuric acid (H_2SO_4, A.R.), and carbon black (CB) were purchased from Chron Chemicals. The ginkgo leaves used in this work were collected from the street in Nanjing, China. The collected leaves were firstly washed with ultrapure water for at least three times and dried in an oven at 80 °C for all night. The dried ginkgo leaves were then smashed by crusher. The obtained powders of ginkgo leaf were with a size of ~300 mesh.

2.2 Synthesis of $Mo_2C\&MoS_2@NSC_x$

0.6 g Ginkgo leaf powders were mixed with AMT (0.6, 0.3, 0.2, 0.15 g) and then grounded for 20 mins. The mixtures were transferred into the tube furnace and calcinated at 900 °C for 5 h in N_2 flow. The as-prepared black samples were denoted as $Mo_2C\&MoS_2$ loaded on N/S co-doped carbon material ($Mo_2C\&MoS_2@NSC_x$, x=1, 2, 3, 4, x represents the weight ratio of Ginkgo leaf powders

and AMT). Solid residue from direct pyrolysis of ginkgo leaves at 900 ^{o}C for 5 h under N_2 protection is called as the N/S co-doped on carbon material (NSC).

2.3 Syntheses of $Mo_2C@NC_3$

0.6 g CB powders were mixed with 0.2 g AMT and then grounding for 20 mins. The mixtures were pyrolysis at 900 ^{o}C for 5 h under N_2 protection. The as-obtained products were named $Mo_2C@NC$.

2.4 Syntheses of $MoS_2@NSC_3$

To avoid the formation of Mo_2C during the pyrolysis, the $MoS_2@NSC$ was prepared via a typical hydrothermal method as reported in Ref. [47] with slightly modification. 0.25 g CH_4N_2S, 0.2 g AMT and 0.6 g CB powders were mixed with 27 mL ultrapure water and ultrasonic mixing for 30 min. The mixture was then transferred into the 50 mL Teflon-lined autoclave and treated at 200 ^{o}C for 18 h. The black precipitates were washed with ultrapure water, ethanol in succession and then dried at 80 ^{o}C in an oven for whole night. Then, the obtained composites were calcination at 900 ^{o}C for 5h with the protection of N_2 flow. The as-prepared sample was named $MoS_2@NSC_3$.

2.4 Materials characterization

The elemental analysis was carried out via Germany THERMO FISHER SCIENTIFIC. The morphology of the as-prepared catalyst was tested by the scanning electron microscopy (SEM, FEI quanta 400FEG). The transmission electron microscopy (TEM, FEI Tecnai 20 electron microscope) and the high-angle annular dark field-scanning transmission electron microscope (HAADF-STEM, FEI TALOSF200S) was employed to further investigate the detailed morphology and analysis the

crystal lattice of hybrid catalysts. The energy-dispersive X-ray spectroscopy-mapping was along with HAADF-STEM to characterize the element distribution. The X-ray powder diffraction (XRD, Bruker D8) equipment was taken to further prove the structural compositions of the as-prepared materials. The surface element composition and chemical state of all catalyst was studied through K-Alpha X-ray photoelectron spectroscopy (XPS, Thermo ESCALAB 250XI). Calibrating with the binding energy using C1s at 284.6 eV. The Raman spectra was conducted using iHR550 Raman microscope (HOR-IBA scientific) at a range of 400~4000 cm^{-1}. The N_2 adsorption experiment on the Quanta 250F and FEI by Brunauer-Emmett Teller (BET) equation at 77.5 K was applied to measure the specific surface area. The ICP Optical emission spectrometer Varian 720-ES (ICP-OES) was employed to analysis the total Mo content of the as-prepared catalysts.

2.5 Electrochemical measurement

The electrochemical tests for HER were conducted on a conventional three-electrode system on CHI 760E electrochemical workstation at room temperature. The graphite rod was selected as the counter electrode. The mercury/mercurous sulfate electrode (MCE, Hg/Hg_2SO_4) was used as the reference electrode in 0.5 M H_2SO_4. The measured potentials were converted potentials vs. reversible hydrogen electrode (RHE) via Eq.(1). All the HER tests were conducted in the saturated N_2 solution via introducing N_2 into the electrolyte solution for at least 30 minutes.

$$E_{vs.RHE} = EvsHg/Hg_2SO_4 + E^{\theta}Hg/Hg_2SO_4 + 0.059\ pH \qquad (1)$$

The glass carbon electrode (GCE, 0.196 cm^{-2}) was served as the working electrode via modified with the catalysts ink. The catalysts ink was obtained by mixed 10 mg of the as-prepared catalysts

with 1000 μL of ethanol/deionized water ($V_{C_2H_5OH}$: V_{H_2O} = 1 : 3) and sonicated for 30 minutes. The well mixed catalysts ink with 10 μL was dropped onto the GC and dried naturally. Then the 10 μL Nafion (5 wt.%) was dropped onto the GCE and dried in the room temperature. The catalysts ink of commercial Pt/C was prepared through the same procedure. For the HER tests, the linear sweep voltammetry (LSV) plots were recorded with 1 mV s^{-1}. And the cyclic voltammetry (CV) tests were performed with the scan rates of 10, 30, 50, 70, 90 mV s^{-1}, respectively.

3 Results and discussion

3.1 Physical-chemistry properties

Before the experiment, the element distributions of raw ginkgo leaves were measured through elemental analysis. The weight ratio of every element was shown in Table S1. The weight ratio of nitrogen (N) and sulfur (S) is 1.070 wt.% and 0.613 wt.% respectively, which can serve as the heteroatom dopants on the carbon frameworks. The scanning electron microscopy (SEM) reveals the morphology of raw ginkgo leaf powders is stack microparticles as shown in Figure S1A. After direct pyrolysis at 900 ^{o}C for 5 h, the microparticles of ginkgo leaves is broken into the smooth sheets (Figure S1B) which induced by the decomposition of organic components. After the AMT is introduced into the pyrolysis process, the carbon sheets are partially destroyed by reacting with AMT. The calcined products are labeled as $Mo_2C\&MoS_2@NSC_x$ (x=1, 2, 3, 4, x represents the weight ratio of Ginkgo leaf powders and AMT). There are many fragments stacked on the spacious carbon flakes as shown in Figure S2. The shattered carbon flakes will benefit for the increase of the specific surface area of hybrid catalysts. However, the excessive AMT will seriously consume the carbon sheets, thus lead to the aggregation of fragments which will cause the reduce of specific

surface area. There may be a best ratio of ginkgo leaves and AMT to obtain a relative higher specific surface area.

Through the N_2 adsorption/desorption tests, the specific surface area and pore structure of $Mo_2C\&MoS_2@NSC_x$ was investigated. As shown in in Figure 1 and Table S2, the specific surface areas of $Mo_2C\&MoS_2@NSC_x$ (x=2, 3, 4) are 189.08, 226.04 and 168.05 $m^2\ g^{-1}$ respectively (Figure 1A) with a large number of nanopores mostly with a size less than 50 nm (Figure 1B). The specific surface area reached to the highest value when the mass ratio of ginkgo leaves and AMT was 3. The AMT promote the crush of carbon flakes derived from ginkgo leaves and thus increase the specific surface areas of hybrid catalysts. As the addition of AMT is equally to the ginkgo leaf powders (x=1), the specific surface areas are sharply reduced (6.12 $m^2\ g^{-1}$). The larger specific surface area and pores structure of $Mo_2C\&MoS_2@NSC_3$ provide more active sites, which will boost catalytic activity. The relatively higher pore volume (Table S2) facilitates the mass transport of reactants to the active sites.

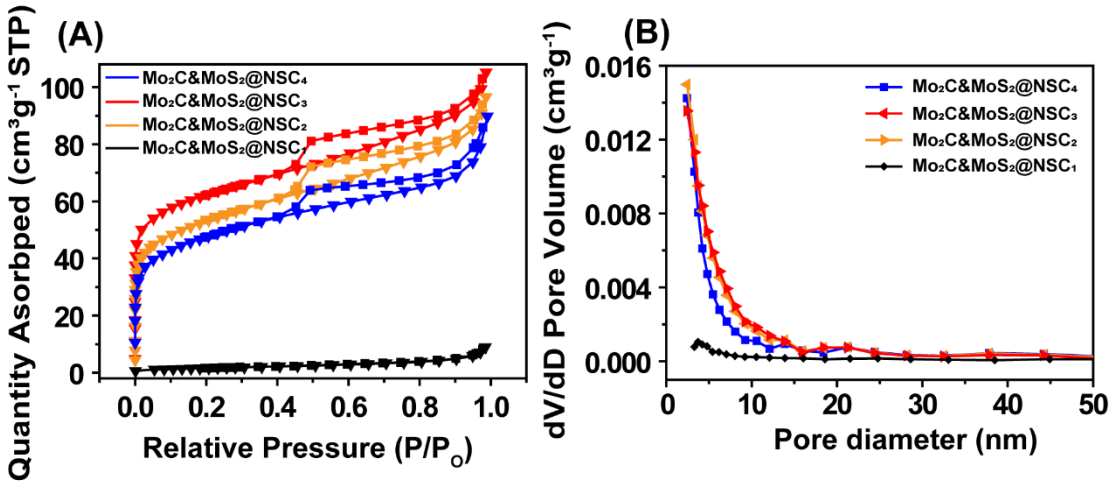

Figure 1 (A) N_2 adsorption/desorption isotherms and **(B)** Pore size distribution curves of $Mo_2C\&MoS_2@NSC_x$ (x=1, 2, 3, 4).

The Raman spectra was used to estimate the graphitization of carbon materials which have further proved the excessive consumption of carbon sheets at a higher addition amount of AMT. As shown in Figure 2A, the two distinct peaks are named *D* band and *G* band, which the *D* band represents the disordered carbon (at 1340 cm^{-1}) and the *G* band indicates the graphite carbon (at 1585 cm^{-1}). Notably, there are not obvious *D* band and *G* band exhibited in the Raman spectra of $Mo_2C\&MoS_2@NSC_1$ because the carbon skeleton is nearly depletion in the conversion process. The value of I_D/I_G for $Mo_2C\&MoS_2@NSC_x$ (x=2, 3, 4) is 0.91, 0.98 and 0.95 respectively. The relative higher value for the $Mo_2C\&MoS_2@NSC_3$ means more structural defects which may enhance the electron exchange and electrochemical activity [10]. The X-ray diffractions (XRD) was employed to confirm the crystal structure of $Mo_2C\&MoS_2@NSC_x$. Besides, as the $Mo_2C\&MoS_2@NSC_3$ own the highest specific surface area and I_D/I_G value, the $Mo_2C@NC_3$ was designed using CB powders to be the control sample and its crystal structure was also investigated. As shown in Figure 2B and Figure S3A, the intensive diffraction at 34.4°, 37.9°, 39.3°, 52.1°, 61.6°, 69.5°, 74.6° and 75.5° corresponding to (1 0 0), (0 0 2), (1 0 1), (1 0 2), (1 1 0), (1 0 3), (1 1 2) and (2 0 1) planes in well-crystallized hexagonal β-Mo_2C (JCPDS No. 35-0787) respectively [18]. For $Mo_2C\&MoS_2@NSC_x$, an additional diffractions peak at 14.2° can be attributed to the (0 0 2) planes in hexagonal MoS_2 (JCPDS No. 37-1492) [48]. With the decrease of AMT, the intensity of MoS_2 peak increases. The peak intensity of $Mo_2C\&MoS_2@NSC_3$ is the strongest, which may be ascribed to the saturation of the combination of Mo and S with the combination of Mo and C, while $Mo_2C\&MoS_2@NSC_4$ exhibit relatively low peaks intensity than $Mo_2C\&MoS_2@NSC_3$ because the insufficient Mo cannot combine more S. Herein, The MoS_2 is originated from the *in-situ* vulcanization of Mo nanoparticles.

The coexist of Mo_2C and MoS_2 will enrich the catalytic sites and accelerate the electron interactions of hybrid catalysts [33, 48]. The ratio of Mo_2C and MoS_2 of $Mo_2C\&MoS_2@NSC_3$ was determined of ~ 34.7:1 via RIR (Reference Intensity Ratio) method (Figure S4), the detailed methods and analyses are shown in supporting information. Furthermore, the total Mo content of $Mo_2C\&MoS_2@NSC_3$ is 453.67 mg/g via the ICP-OES tests. Therefore, the content of Mo_2C and MoS_2 of $Mo_2C\&MoS_2@NSC_3$ is 440.96 mg/g and 12.70 mg/g, respectively. In addition, the chemical stats of Mo-based compounds and N/S elements dispersed on the surface played crucial role in the electrocatalytic activity. The surface compositions of the $Mo_2C\&MoS_2@NSC_3$ and Mo_2C@NC was further analysis via X-ray photoelectron spectroscopy (XPS).

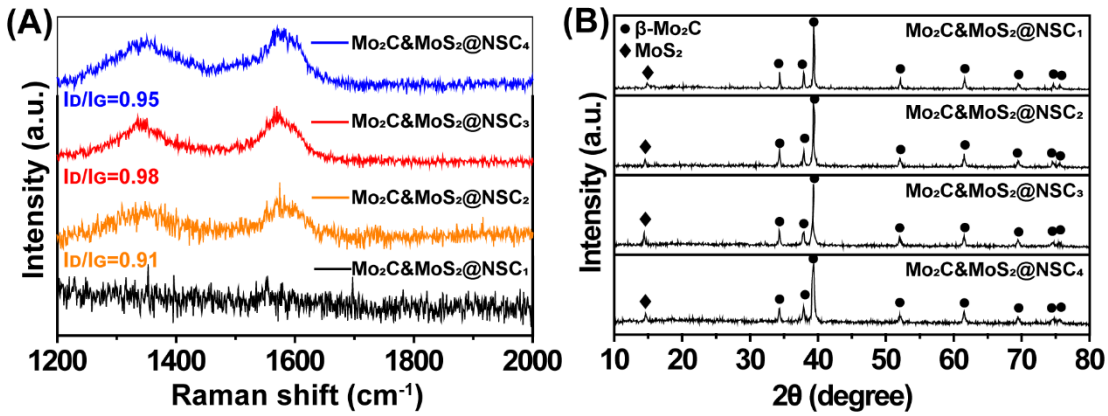

Figure 2 (A) Raman and **(B)** XRD patterns of $Mo_2C\&MoS_2@NSC_x$ (x=1, 2, 3, 4).

The full spectrum (Figure 3A) indicates that the $Mo_2C\&MoS_2@NSC_3$ consisted of C, N, O, S, Mo elements. Fitted Mo 3d spectrum (Figure 3B) indicates the existence of Mo^{4+} and Mo^{6+} species, the Mo^{4+} is originated from the MoS_2 and oxide Mo_2C. The Mo^{4+} and Mo^{6+} is attributed to the molybdenum trioxide resulting from surface oxidation of Mo_2C. The peaks at 228.86 and 232.95 eV indicate the Mo^{4+} $3d_{5/2}$ and Mo^{4+} $3d_{3/2}$ states of Mo, respectively [49-51], which are shifted

toward higher BE after the formation of the MoS_2. This may be associated with the higher electronegativity of S compared to C. The fine spectrum of the Mo 3d was deconvolved to further analysis the surface chemical states of Mo atoms. As shown in Figure S5, there are also two peaks located at 229.25 and 231.75 eV in the fitted Mo 3d fine spectrum of $Mo_2C\&MoS_2@NSC_3$ compared with $Mo_2C@NC_3$. These two peaks indicated the Mo $^{4+}$ $3d_{5/2}$ and Mo $^{5+}$ $3d_{5/2}$ [52], which is also resulted from the surface oxidation of Mo_2C. The full width at half maximum of C oxidation states is decreased from 1.42 to 1.21 eV after growing MoS_2 on ginkgo leaves derived carbon matrix, which indicates a higher spin coupling effect between Mo and C atoms in $Mo_2C\&MoS_2@NSC_3$ catalysts (Figure S6). While for S 2p fine spectrum (Figure 3C), the two peaks at 161.64 and 162.92 eV corresponding to the S $2p_{3/2}$ and S $2p_{1/2}$ states of S, respectively [48]. It confirms that the S was transformed into the dopants in carbon matrix and simultaneously combined with Mo. For $Mo_2C@NC_3$, there is no characteristic peak of S. Besides, there are also no obvious N 1 peaks because the N atoms only came from the AMT which caused the extremely low N dopants (only 1.60% in Table S3) in $Mo_2C@NC_3$. The content of N in $Mo_2C\&MoS_2@NSC_3$ is as high as 14.44%. By comparing the N 1 spectrum of the $Mo_2C\&MoS_2@NSC_3$ and $Mo_2C@NC_3$, the four peaks of fitted N 1 spectrum of $Mo_2C\&MoS_2@NSC_3$ at 396.51 eV, 398.36 eV, 399.48 eV and 401.26 eV in Figure 3D indicating the existence of N-Mo, pyridinic N, pyrrolic N and graphite N, respectively [49]. The states of N element in $Mo_2C@NC_3$ sample are similar to that in $Mo_2C\&MoS_2@NSC_3$ (Figure S7), but the BEs of N elements in $Mo_2C\&MoS_2@NSC_3$ are obviously negatively shift due to the presence of S, which influence the electronic coupling effect between C and Mo. As shown in Figure 3B, the BEs for Mo^{4+} and Mo^{6+} of $Mo_2C\&MoS_2@NSC_3$ is positively shifted compared with $Mo_2C@NC_3$, which suggest that the electron transfer from Mo to the S atoms due to its high

electronegativity. The electronegativity of N atoms is higher than S atoms, the electron enrich in the surface of NSC will be captured by the N atoms, thus cause the negatively shift of BEs of N elements. Such results confirm the strong electron interaction of the $Mo_2C\&MoS_2@NSC_3$, which can enhance the HER activity. Therefore, the XPS analysis proves the possible N- and S-doping in carbon matrix and the successful synthesis of Mo_2C and MoS_2. The N/S dopants with higher electronegativity into the carbon lattice will lead to the destroy of electric neutrality and the charge density of carbon atoms, thus cause the defects of disordered carbon.

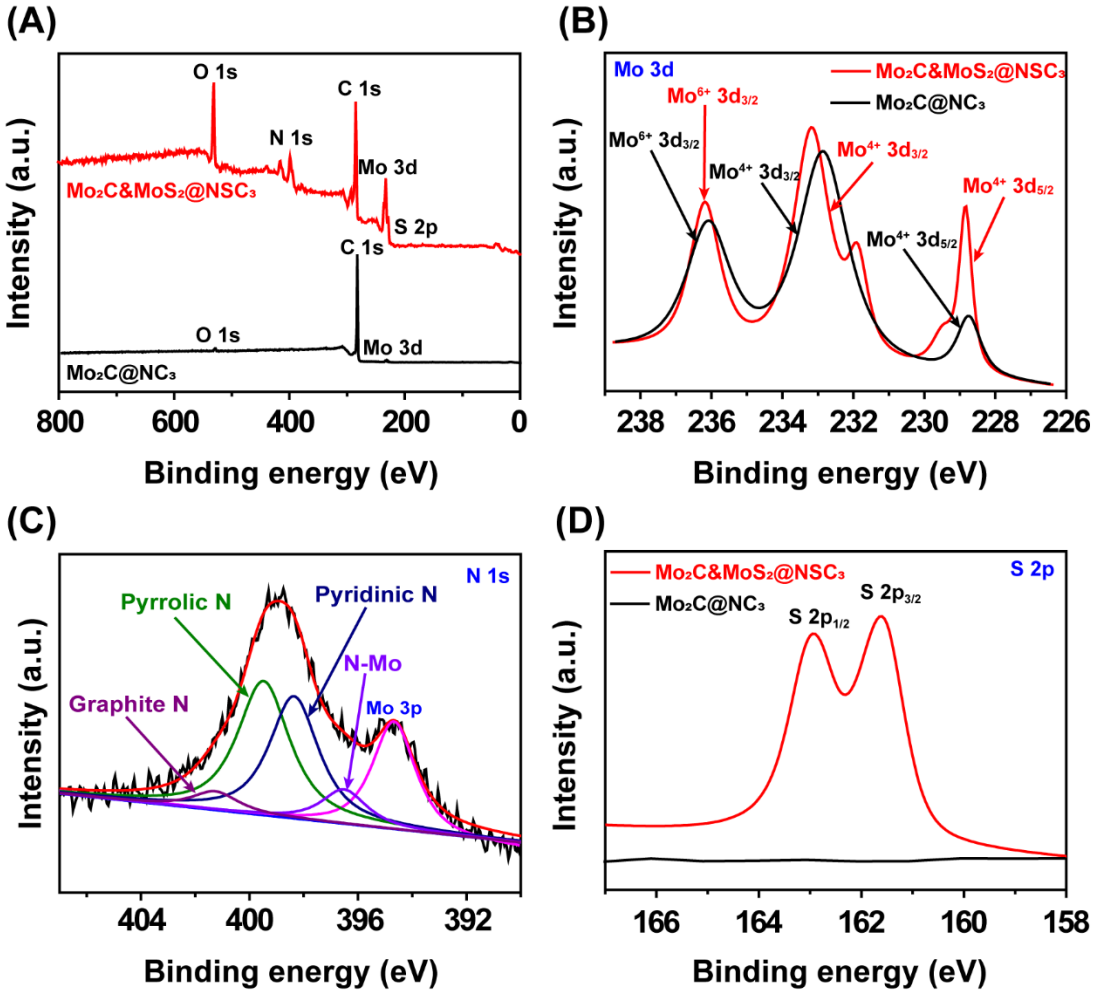

Figure 3 (A) Full XPS spectra of $Mo_2C@NC_3$ and $Mo_2C\&MoS_2@NSC_3$. **(B)** Mo 4d and **(C)** S 2p XPS scan spectra for $Mo_2C@NC_3$ and $Mo_2C\&MoS_2@NSC_3$. **(D)** N 1s XPS spectra for $Mo_2C\&MoS_2@NSC_3$.

Transmission electron microcopy (TEM) and high-resolution transmission electron microcopy (HRTEM) were carried out to in-depth analysis the structure of $Mo_2C\&MoS_2@NSC_3$. As shown in Figure 4A-C, it can be seen that the Mo nanoparticles disperse on the surface of carbon flakes homogenously with a size range from 5 to 20 nm. From the HRTEM images (Figure 4D) of $Mo_2C\&MoS_2@NSC_3$, it shows that there are two different crystal structures inside. The lattice plane distance of 0.15 nm corresponds to the (1 1 0) plane of Mo_2C, and 0.16 nm accords with the (1 1 0) plane of MoS_2, which was well corresponding to the XRD results. In addition, the element distribution of Mo, C, S, N, O was revealed by HAADF-STEM mapping images (Figure 4E). It is worth noting that the S content is highly overlapped with the region of Mo, which is consistent with the formation of MoS_2. In addition, a small amount of S is doped into the carbon sheet. The successful doping of S and N would change the electrical neutrality of carbon and thus promote the charge transfer capability [40, 53]. Furthermore, the Mo_2C and MoS_2 have more moderate hydrogen boding energy which would facilitate the adsorption and desorption of intermediate media, thus resulted in more fast kinetic process [48].

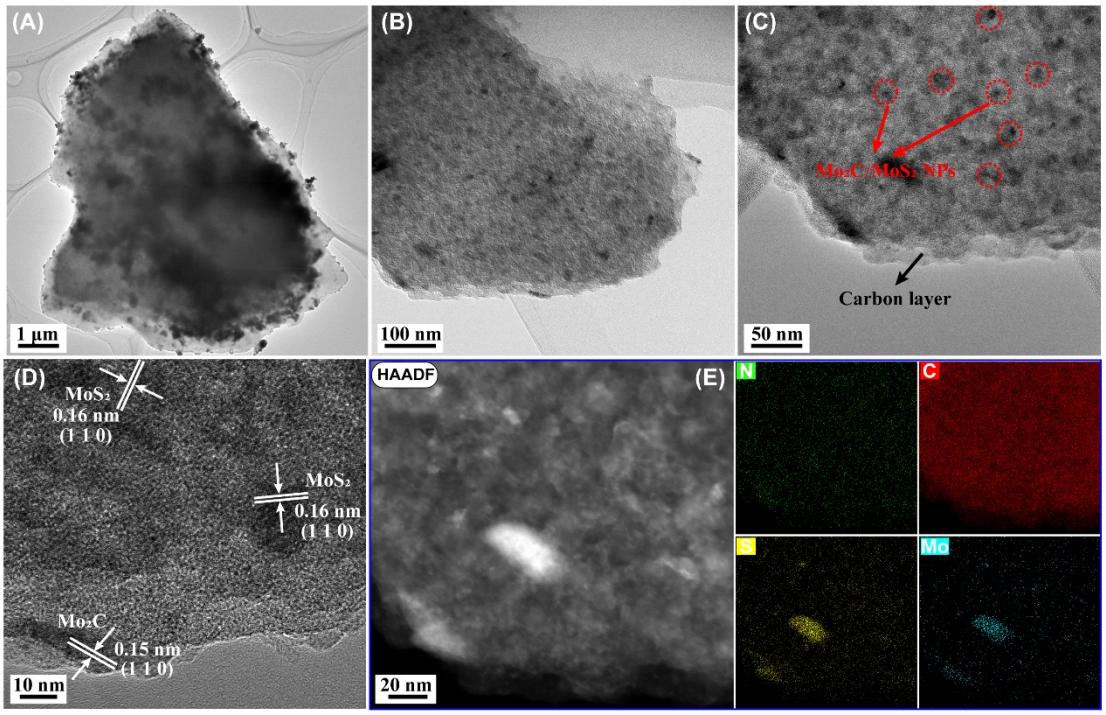

Figure 4 (A, B, C) TEM image, **(D)** HRTEM images of $Mo_2C\&MoS_2@NSC_3$. **(E)** STEM image and the element mapping image of N, C, S and Mo elements of $Mo_2C\&MoS_2@NSC_3$.

3.2 HER performance in acid electrolyte

The HER performance of the as-prepared samples and benchmark 20% commercial Pt/C catalyst in 0.5 M H_2SO_4 was firstly explored. Figure 5A displayed the linear polarization curves (LSV) plots with a scan rate of 1 mV S^{-1}. As one can see, the commercial Pt/C exhibits anticipated electrocatalytic performance with a near zero onset potential, together with 35 mV at standard current of 10 mA cm^{-2}. The overpotential of $Mo_2C\&MoS_2@NSC_x$ (x=1, 2, 3, 4) to drive the current density to 10 mA cm^{-2} was 331, 226, 209, and 220 mV (η_{10}), respectively. As expected, the $Mo_2C\&MoS_2@NSC_3$ has the best electrocatalytic activity among the $Mo_2C\&MoS_2@NSC_x$, and is much better than that of $Mo_2C@NC_3$ (713 mV) and NSC (> 1100 mV). The introduction of Mo_2C and MoS_2 which can serve as the active sites can enhance the activity of ginkgo leaves derived

carbon for catalytic HER. Meanwhile, the addition amount of AMT seriously affects the HER performance of the as-synthesized electrocatalysts. Especially, the excessive addition of AMT will result in the depletion of carbon skeleton and cause the decrease of catalytic activity. The $MoS_2@NSC_3$ is also prepared and its crystal structure is identified via XRD (Figure S3B). The overpotential for $Mo_2S@NSC_3$ to afford 10 mA cm^{-2} current density is 498 mV, which is better than $Mo_2C@NC_3$, but worse than $Mo_2C\&MoS_2@NSC_3$. In Figure 5B and S8, the corresponding Tafel slopes for $Mo_2C\&MoS_2@NSC_x$ (x=1, 2, 3, 4) $MoS_2@NSC_3$ and $Mo_2C@NC_3$ are 250.8 mV dec^{-1}, 110.5 mV dec^{-1}, 85.5 mV dec^{-1}, 111.6 mV dec^{-1}, 129.7 mV dec^{-1} and 208.6 mV dec^{-1}, respectively. The Tafel slope values of $Mo_2C\&MoS_2@NSC_3$ indicate its likely occur through the Volmer-Heyrovsky mechanism. Moreover, the $Mo_2C\&MoS_2@NSC_3$ has a C_{dl} value of 10.72 mF cm^{-2}, which is far higher than $Mo_2C\&MoS_2@NSC_1$ (6.04 mF cm^{-2}), $Mo_2C\&MoS_2@NSC_2$ (6.39 mF cm^{-2}), $Mo_2C\&MoS_2@NSC_4$ (9.91 mF cm^{-2}), $MoS_2@NSC_3$ (5.62 mF cm^{-2}) and $Mo_2C@NC_3$ (4.97 mF cm^{-2}) (Figure S9 and 5C), indicating that $Mo_2C\&MoS_2@NSC_3$ exhibits a larger active surface area. The HER performance of the as-prepared $Mo_2C\&MoS_2@NSC_3$ is compared with the reported Mo_2C or MoS_2 based electrocatalysts as shown in Table S4. It is observed that the HER activity of the as-obtained electrocatalysts can contend with other Mo-based electrocatalysts. Besides, the remarkable stability of $Mo_2C\&MoS_2@NSC_3$ within 15 h of continuous operation in a 0.5 M H_2SO_4 solution, was proved by a chronoamperometric test.

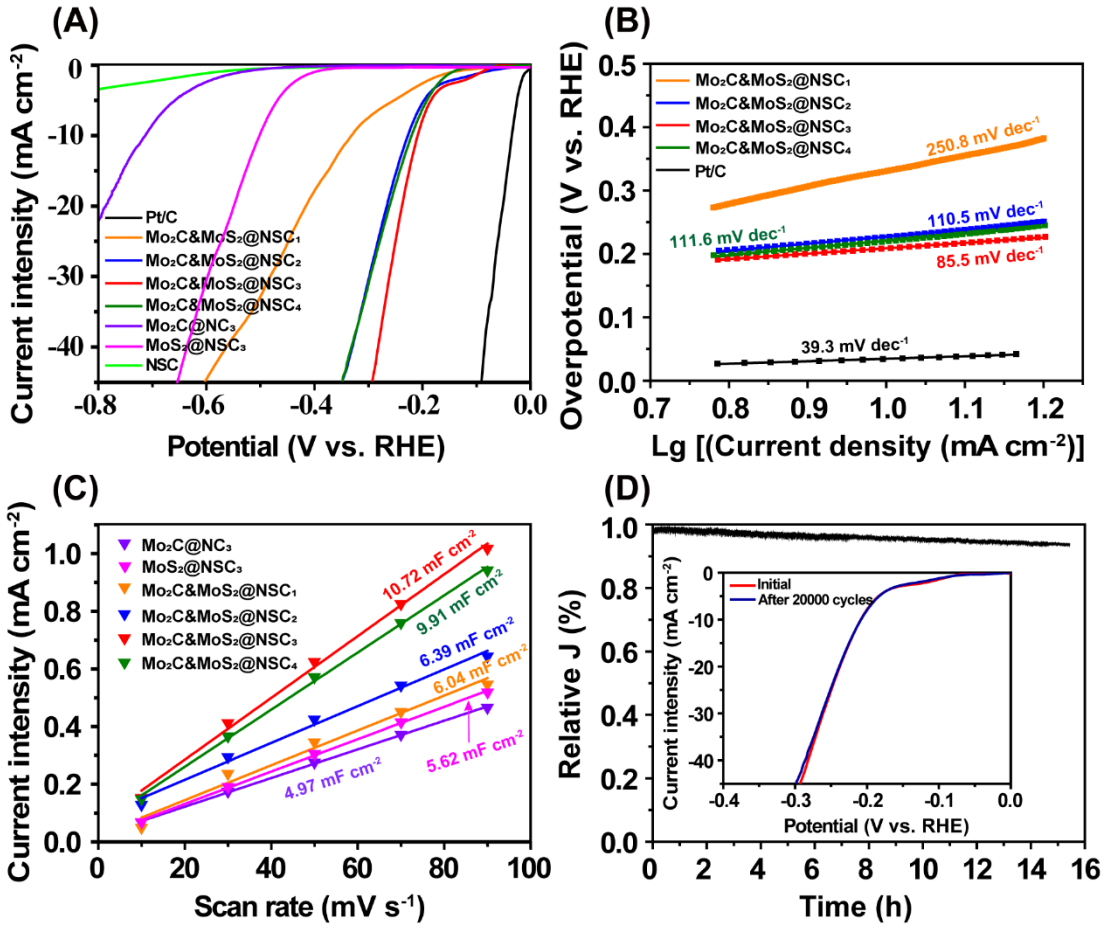

Figure 5 (A) LSV curves of NSC, $Mo_2C@NC_3$ and $Mo_2C\&MoS_2@NSCx$ (x=1, 2, 3, 4) in 0.5 M H_2SO_4 electrolyte. **(B)** Corresponding Tafel curves derived from **(A)**. **(C)** C_{dl} stands for ECSA of the five electrocatalysts. **(H)** Durability test of $Mo_2C\&MoS_2@NSC_3$.

As manifested in Figure 5D, there is a negligible current decay (< 10%) and almost invariable catalytic activity after 2000 cycles (Figure 5D inset), which indicates the superior stability of $Mo_2C\&MoS_2@NSC_3$. After stability tests, the catalysts were recycled to employ the XRD, XPS, SEM and TEM testing to further prove the stability of the $Mo_2C\&MoS_2@NSC_3$. The crystal structure of $Mo_2C\&MoS_2@NSC_3$ was firstly identified via XRD (Figure S10). All the diffraction peaks are matched well with original $Mo_2C\&MoS_2@NSC_3$. The same BEs of Mo 3d, N 1s, S 2p, (Figure S11 A-D) are found for the recycled catalysts after HER tests, which demonstrate that there

is nearly no change in the surface valence sate of various species of $Mo_2C\&MoS_2@NSC_3$. In addition, representative SEM image of the surface after i-t tests are shown in Figure S12 A, which suggests that the morphology of the accumulated fragments on carbon matrix have not changed during the stability tests. As shown in the TEM image (Figure S12 B), the Mo_2C and MoS_2 nanoparticles are homogeneously dispersed on the carbon support. Such observations indicate no evidence of any phase transformation during the stability tests, suggest the robust stability of the as-prepared catalysts.

Utilizing the microstructure of ginkgo leaves and its characteristics of being rich in N and S elements, $Mo_2C\&MoS_2@NSC_3$ catalyst was synthesized by mixing and calcining ginkgo leaves with AMT in one step. There are three possible explanations for the high catalysis characteristics our synthesized $Mo_2C\&MoS_2@NSC_3$ catalyst: (1) ginkgo leaves not only serve as the N/S doped carbon supports, but also served as the reactants to combine with Mo to *in-situ* form Mo_2C and MoS_2, which have been proved to favor the electron interactions. Meanwhile, the synergistic effect of $Mo_2C\&MoS_2$ with NSC make $Mo_2C\&MoS_2@NSC_3$ show an excellent HER performance, (2) the carbon structural defects which are beneficial for electrochemical reactions, (3) the larger specific surface area, pores structure and high pore volume of $Mo_2C\&MoS_2@NSC_3$ are conducive to the uniform dispersion of active components, and play a positive role in reducing the size of active centers and preventing sintering agglomeration of active components, thus leading to high HER activity. Our study shed light up a universal and effective way to fabricate dual phase of Mo-based carbon catalysts derived from ginkgo leaves as the electrocatalysts with high-active, long-term stability and cost-effective for HER.

4 Conclusions

In summary, an environment-friendly one-pot protocol to prepare $Mo_2C\&MoS_2$ loaded on N/S co-doped carbon nanosheets was designed by using the common biomass waste-ginkgo leaves. Benefited from the N and S contents of ginkgo leaves, the dopants of N and S atoms was *in-situ* introduced into the carbon skeleton without additive agents. The Mo_2C and MoS_2 was resulted from the reactions between Mo and C (or S) in the pyrolysis process. The Mo_2C and MoS_2 as the active sites and N/S co-doped carbon matrix endows the hybrids catalyst with superior activity to catalytic H_2 evolution. During the HER tests in 0.5 M H_2SO_4, the $Mo_2C\&MoS_2@NSC_3$ only needs 209 mV to drive the cathodic current density to 10 mA cm^{-2}, as well as a relatively low Tafel slope of 85.5 mV dec^{-1} and superb durability. The hybrid electrocatalysts was demonstrated to be potential to serve as the HER catalysts. In addition, it also offers an efficient way to utilize the waste biomass which was rich in N and S contents.

Declaration of competing interest

The authors declare that they have no known competing financial interests or personal relationships that could have appeared to influence the work reported in this paper.

Acknowledgements

The authors gratefully acknowledge the support of National Natural Science Foundation (51878145 and 51861145102), and Jiangsu Provincial Key Research and Development Program (BE2020114).

References

[1] Khan R, Mehran MT, Baig MM, Sarfraz B, Naqvi SR, K. Niazi MB, et al. 3D hierarchical heterostructured LSTN@NiMn-layered double hydroxide as a bifunctional water splitting electrocatalyst for hydrogen production. Fuel 2021;285:119174.

[2] Dauptain K, Schneider A, Noguer M, Fontanille P, Escudie R, Carrere H, et al. Impact of microbial inoculum storage on dark fermentative H_2 production. Bioresour Technol 2021; 319:124234.

[3] Gao N, Chen K, Lai X, Quan C. Catalytic steam reforming of real tar under high-efficiency Ni/USY catalyst for H_2 production. Fuel 2021;306:121676.

[4] Zhang Z, Qin C, Ou Z, Xia H, Ran J, Wu C. Experimental and thermodynamic study on sorption-enhanced steam reforming of toluene for H_2 production using the mixture of Ni/perovskite-CaO. Fuel 2021;305:121447.

[5] Hoang VC, Gomes VG, Dinh KN. Ni- and P-doped carbon from waste biomass: A sustainable multifunctional electrode for oxygen reduction, oxygen evolution and hydrogen evolution reactions. Electrochim Acta 2019;314:49-60.

[6] Jiang L, Seong Y-H, Han SO, Kim H, Kim HH, Foord JS. Nickel treatment of biomass-derived nanocarbon for energy devices. Carbon 2018;130:724-9.

[7] Zhang L, Roling LT, Wang X, Vara M, Chi M, Liu J, Sang-II C, et al. Platinum-based nanocages with subnanometer-thick walls and well-defined, controllable facets. Science 2015;349(6246):412-6.

[8] Greeley J, Jaramillo TF, Bonde J, Chorkendorff IB, Norskov JK. Computational high-throughput screening of electrocatalytic materials for hydrogen evolution. Nat Mater

2006;5(11):909-13.

[9] Hoang VC, Dinh KN, Gomes VG. Hybrid Ni/NiO composite with N-doped activated carbon from waste cauliflower leaves: A sustainable bifunctional electrocatalyst for efficient water splitting. Carbon 2020;157:515-24.

[10] Xu L-H, Zeng H-B, Zhang X-J, Cosnier S, Marks RS, Shan D. Highly active $M_2P_2O_7$@NC (M = Co and Zn) for bifunctional electrocatalysts for ORR and HER. J Catal 2019;377:20-7.

[11] Xu L-H, Zhang S-L, Guo S-Y, Zhang X-J, Cosnier S, Marks RS, et al. ATMP derived cobalt-metaphosphate complex as highly active catalyst for oxygen reduction reaction. J Catal 2020;387:129-37.

[12] Wu D, Chen D, Zhu J, Mu S. Ultralow Ru Incorporated Amorphous Cobalt-Based Oxides for High-Current-Density Overall Water Splitting in Alkaline and Seawater Media. Small 2021;e2102777.

[13] Wei C, Sun Y, Scherer GG, Fisher AC, Sherburne M, Ager JW, et al. Surface Composition Dependent Ligand Effect in Tuning the Activity of Nickel-Copper Bimetallic Electrocatalysts toward Hydrogen Evolution in Alkaline. J Am Chem Soc 2020;142(17):7765-75.

[14] Yang L, Zhou W, Jia J, Xiong T, Zhou K, Feng C, et al. Nickel nanoparticles partially embedded into carbon fiber cloth via metal-mediated pitting process as flexible and efficient electrodes for hydrogen evolution reactions. Carbon 2017;122:710-7.

[15] Yin J, Fan Q, Li Y, Cheng F, Zhou P, Xi P, et al. Ni-C-N Nanosheets as Catalyst for Hydrogen Evolution Reaction. J Am Chem Soc 2016;138(44):14546-9.

[16] Zhang TQ, Liu J, Huang LB, Zhang XD, Sun YG, Liu XC, et al. Microbial-Phosphorus-Enabled Synthesis of Phosphide Nanocomposites for Efficient Electrocatalysts. J Am Chem Soc 2017;139(32):11248-53.

[17] Fakayode OA, Yusuf BA, Zhou C, Xu Y, Ji Q, Xie J, et al. Simplistic two-step fabrication of porous carbon-based biomass-derived electrocatalyst for efficient hydrogen evolution reaction. Energy Convers Manage 2021;227:113628.

[18] An K, Xu X, Liu X. Mo2C-Based Electrocatalyst with Biomass-Derived Sulfur and Nitrogen Co-Doped Carbon as a Matrix for Hydrogen Evolution and Organic Pollutant Removal. ACS Sustain Chem Eng 2017;6(1):1446-55.

[19] Zhu J, Hu L, Zhao P, Lee LYS, Wong KY. Recent Advances in Electrocatalytic Hydrogen Evolution Using Nanoparticles. Chem Rev 2020;120(2):851-918.

[20] Furimsky E. Metal carbides and nitrides as potential catalysts for hydroprocessing[J]. Appl Catal A 2003;240(1-2):1-28.

[21] Gao Q, Zhang C, Wang S, Shen W, Zhang Y, Xu H, et al. Preparation of supported Mo(2)C-based catalysts from organic-inorganic hybrid precursor for hydrogen production from methanol decomposition. Chem Commun 2010;46(35):6494-6.

[22] Weidman MC, Esposito DV, Hsu Y-C, Chen JG. Comparison of electrochemical stability of transition metal carbides (WC, W_2C, Mo_2C) over a wide pH range. J Power Sources 2012;202:11-7.

[23] Youn DH, Han S, Kim JY, Kim JY, Park H, Choi SH, Lee JS, Highly active and stable hydrogen evolution electrocatalysts based on molybdenum compounds on carbon nanotube-graphene hybrid support. ACS Nano 2014;8(5):5164-73.

[24] Tsai C, Abild-Pedersen F, Norskov JK. Tuning the MoS(2) edge-site activity for hydrogen evolution via support interactions. Nano Lett 2014;14(3):1381-7.

[25] Liao L, Zhu J, Bian X, Zhu L, Scanlon MD, Girault HH, et al. MoS_2 Formed on Mesoporous Graphene as a Highly Active Catalyst for Hydrogen Evolution. Adv Funct Mater 2013;23(42):5326-33.

[26] Xie J, Zhang J, Li S, Grote F, Zhang X, Zhang H, et al. Controllable disorder engineering in oxygen-incorporated MoS_2 ultrathin nanosheets for efficient hydrogen evolution. J Am Chem Soc 2013;135(47):17881-8.

[27] Humagain G, MacDougal K, MacInnis J, Lowe JM, Coridan RH, MacQuarrie S, et al. Highly Efficient, Biochar-Derived Molybdenum Carbide Hydrogen Evolution Electrocatalyst. Adv Energy Mater 2018;8(29):1801461.

[28] Park S-K, Chung DY, Ko D, Sung Y-E, Piao Y. Three-dimensional carbon foam/N-doped graphene@MoS_2 hybrid nanostructures as effective electrocatalysts for the hydrogen evolution reaction. J Mater Chem A 2016;4(33):12720-5.

[29] McAteer D, Gholamvand Z, McEvoy N, Harvey A, O'Malley E, Duesberg GS, et al. Thickness Dependence and Percolation Scaling of Hydrogen Production Rate in MoS_2 Nanosheet and Nanosheet-Carbon Nanotube Composite Catalytic Electrodes. ACS Nano 2016;10(1):672-83.

[30] Murthy AP, Theerthagiri J, Madhavan J, Murugan K. Highly active MoS_2/carbon electrocatalysts for the hydrogen evolution reaction - insight into the effect of the internal resistance and roughness factor on the Tafel slope. Phys Chem Chem Phys 2017;19(3):1988-98.

[31] Zhang K, Zhao Y, Fu D, Chen Y. Molybdenum carbide nanocrystal embedded N-doped carbon nanotubes as electrocatalysts for hydrogen generation. J Mater Chem A 2015;3(11):5783-8.

[32] Li JS, Wang Y, Liu CH, Li SL, Wang YG, Dong LZ, et al. Coupled molybdenum carbide and reduced graphene oxide electrocatalysts for efficient hydrogen evolution. Nat Commun 2016;7:11204.

[33] Chi J-Q, Shang X, Lu S-S, Dong B, Liu Z-Z, Yan K-L, et al. Mo_2C@NC@MoSx porous nanospheres with sandwich shell based on MoO_4^{2-}-polymer precursor for efficient hydrogen evolution in both acidic and alkaline media. Carbon 2017;124:555-64.

[34] Jeon J, Park Y, Choi S, Lee J, Lim SS, Lee BH, et al. Epitaxial Synthesis of Molybdenum Carbide and Formation of a Mo_2C/MoS_2 Hybrid Structure via Chemical Conversion of Molybdenum Disulfide. ACS Nano 2018;12(1):338-46.

[35] Anjum MAR, Lee MH, Lee JS. BCN network-encapsulated multiple phases of molybdenum carbide for efficient hydrogen evolution reactions in acidic and alkaline media. J Mater Chem A 2017;5(25):13122-9.

[36] Tjandra R, Liu W, Lim L, Yu A. Melamine based, n-doped carbon/reduced graphene oxide composite foam for Li-ion Hybrid Supercapacitors. Carbon 2018;129:152-8.

[37] Yang C, Jin H, Cui C, Li J, Wang J, Amine K, et al. Nitrogen and sulfur co-doped porous carbon sheets for energy storage and pH-universal oxygen reduction reaction. Nano Energy 2018;54:192-9.

[38] Zhang K, Zhao Y, Zhang S, Yu H, Chen Y, Gao P, et al. MoS_2 nanosheet/Mo_2C-embedded N-doped carbon nanotubes: synthesis and electrocatalytic hydrogen evolution performance.

J Mater Chem A 2014;2(44):18715-9.

[39] Liu X, Zhou W, Yang L, Li L, Zhang Z, Ke Y, et al. Nitrogen and sulfur co-doped porous carbon derived from human hair as highly efficient metal-free electrocatalysts for hydrogen evolution reactions. J Mater Chem A 2015;3(16):8840-6.

[40] Zhou Y, Leng Y, Zhou W, Huang J, Zhao M, Zhan J, et al. Sulfur and nitrogen self-doped carbon nanosheets derived from peanut root nodules as high-efficiency non-metal electrocatalyst for hydrogen evolution reaction. Nano Energy 2015;16:357-66.

[41] Prabu N, Saravanan RSA, Kesavan T, Maduraiveeran G, Sasidharan M. An efficient palm waste derived hierarchical porous carbon for electrocatalytic hydrogen evolution reaction. Carbon 2019;152:188-97.

[42] Gao J, Chu X, He C, Yin Z, Lu H, Li X, et al. Biomass-derived carbon for ORR: pine needles as a single source for efficient carbon electrocatalyst. J Appl Electrochem 2020;50(12):1257-67.

[43] Li X, Guan BY, Gao S, Lou XW. A general dual-templating approach to biomass-derived hierarchically porous heteroatom-doped carbon materials for enhanced electrocatalytic oxygen reduction. Energy Environ Sci 2019;12(2):648-55.

[44] Zeng L, Li X, Fan S, Mu J, Qin M, Wang X, et al. Seaweed-Derived Nitrogen-Rich Porous Biomass Carbon as Bifunctional Materials for Effective Electrocatalytic Oxygen Reduction and High-Performance Gaseous Toluene Absorbent. ACS Sustain Chem Eng 2019;7(5):5057-64.

[45] Chen M, Wang S, Zhang H, Zhang P, Tian Z, Lu M, et al. Intrinsic defects in biomass-derived carbons facilitate electroreduction of CO_2. Nano Res 2020;13(3):729-35.

[46] Yao P, Qiu Y, Zhang T, Su P, Li X, Zhang H. N-Doped Nanoporous Carbon from Biomass as a Highly Efficient Electrocatalyst for the CO_2 Reduction Reaction. ACS Sustain Chem Eng 2019;7(5):5249-55.

[47] Xie X, Makaryan T, Zhao M, Van Aken KL, Gogotsi Y, Wang G. MoS_2 Nanosheets Vertically Aligned on Carbon Paper: A Freestanding Electrode for Highly Reversible Sodium-Ion Batteries. Adv Energy Mater 2016;6(5):1502161.

[48] Yang S, Wang Y, Zhang H, Zhang Y, Liu L, Fang L, et al. Unique three-dimensional $Mo_2C@MoS_2$ heterojunction nanostructure with S vacancies as outstanding all-pH range electrocatalyst for hydrogen evolution. J Catal 2019;371:20-6.

[49] Chen YY, Zhang Y, Jiang WJ, Zhang X, Dai Z, Wan LJ, et al. Pomegranate-like N,P-Doped Mo2C@C Nanospheres as Highly Active Electrocatalysts for Alkaline Hydrogen Evolution. ACS Nano 2016;10(9):8851-60.

[50] Geng D, Zhao X, Chen Z, Sun W, Fu W, Chen J, et al. Direct Synthesis of Large-Area 2D Mo2 C on In Situ Grown Graphene. Adv Mater Interfaces 2017, 29(35):1700072.

[51] Tiwari AP, Yoon Y, Novak TG, Azam A, Lee M, Lee SS, et al. Lattice Strain Formation through Spin-Coupled Shells of MoS_2 on Mo_2C for Bifunctional Oxygen Reduction and Oxygen Evolution Reaction Electrocatalysts. Adv Mater Interfaces 2019;6(22):1900948.

[52] Murugappan K, Anderson EM, Teschner D, Jones TE, Skorupska K, Román-Leshkov Y. Operando NAP-XPS unveils differences in MoO_3 and Mo_2C during hydrodeoxygenation. Nat Catal 2018;1(12):960-7.

[53] Ito Y, Cong W, Fujita T, Tang Z, Chen M. High catalytic activity of nitrogen and sulfur co-doped nanoporous graphene in the hydrogen evolution reaction. Angew Chem Int Ed

2015;54(7):2131-6.